Full-wave analysis of imaging by the Pendry-Ramakrishna stackable lens

A. V. Dorofeenko,[1] A. A. Lisyansky,[2] A. M. Merzlikin,[1] and A. P. Vinogradov[1,*]
[1]*Institute of Theoretical and Applied Electromagnetism, Russian Academy of Sciences, 125412 Moscow, Izhorskaya, 13/19, Russia*
[2]*Department of Physics, Queens College of the City University of New York, Flushing, New York 11367, USA*
(Received 10 April 2006; published 30 June 2006)

We perform a full-wave analysis of a stackable lens proposed in a recent paper [Ramakrishna *et al.*, J. Mod. Optics **50**, 1419 (2003)]. This lens was suggested for improving subwavelength imaging and can be obtained by splitting a single-layer lens into a set of thinner layers. Our analysis shows that (i) such a lens, which forms a one-dimensional photonic crystal (PC), is a resonator cavity for traveling Bloch waves that cannot leave this PC resonator due to total internal reflection; (ii) imaging is possible outside the band gaps only and no imaging can be achieved in the vicinity of the eigenstates of the PC resonator as well as near the state associated with the excitation of the volume plasmon; (iii) the expected advantage is due to thinning the layers, which results in shifting of both the band edge and the eigenstates toward higher values of the wave number; and (iv) a single-layer lens has the broadest working range compared to a stackable lens with the same elementary layer thickness.

DOI: 10.1103/PhysRevB.73.235126 PACS number(s): 78.20.Ci, 42.30.Wb, 42.70.Qs, 73.20.Mf

I. INTRODUCTION

In 1968, Veselago[1] showed that a medium with both negative permittivity and permeability (a left-handed medium) exhibited a negative refraction as predicted in Ref. 2. The most pronounced property of the left-handed medium, predicted by Veselago, is that a slab made of such a material acts as a focusing lens, producing a real image of a source placed in front of the slab. In 2000 Pendry[3] showed that an image produced by the Veselago lens consists not only of far field harmonics but also of near field harmonics of the source. Thus, it has become possible to overcome the Rayleigh limit in imaging employing surface plasmon-magnon resonances excited by the near fields.[3,4] As a result, a slab of thickness L at a distance l_2 behind the lens perfectly restores the image of the source placed at a distance l_1 in front of the lens, where these distances are related by the equation $l_1+l_2=L$.[3] The latter fact is very important in photolithography because the left-handed slab shifts the perfect image from a stencil-photoresist interface to deeper inside the photoresist, making the performance of the ultimate mask better.[5,6]

However, a left-handed medium is still not known in optics; therefore, Pendry[3] suggested using a medium (e.g., silver) with negative permittivity only for optical applications. Such a medium does not exhibit negative refraction, and space harmonics with small values of the transverse wave number k_x are not focused and do not create an image. Nevertheless, in a slab with $\varepsilon_2=-1$, $\mu_2=1$ placed in the xy plane, the TM space harmonics with high values of k_x are still amplified by the plasmon resonance, which makes the resolution of small details possible.

To describe wave propagation through such a slab for high values of k_x ($k_0/k_x \ll 1$, $k_0=\omega/c$), one can use an electrostatic approximation.[3] In the Maxwell equations, one can ignore the time derivatives compared to the spatial ones. In this case, the values of normal components of the wave vectors in vacuum,

$$k_{z1}=(k_0^2-k_x^2)^{1/2}\approx ik_x, \tag{1a}$$

and in the negative-epsilon medium,

$$k_{z2}=(\varepsilon_2\mu_2 k_0^2-k_x^2)^{1/2}\approx ik_x, \tag{1b}$$

as well as the corresponding impedance values for the TM wave,

$$\zeta_1=\frac{k_z}{k_0}\approx\frac{ik_x}{k_0},\quad \zeta_2=\frac{k_z}{\varepsilon_2 k_0}\approx\frac{ik_x}{\varepsilon_2 k_0}, \tag{2}$$

no longer depend on the permeability. Therefore, the sign of μ is immaterial and the TM space harmonics are treated by this lens in the same way as by a slab of left-handed material. This note does not concern the TE-polarized waves, for which $\zeta=\mu k_0/k_z\approx -i\mu k_0/k_x$. Further, we will consider the case of the TM polarization.

To study the lens, we decompose the electromagnetic field into plane waves and employ the transfer function method.[4,7] For example, for the TM polarization this method implies that the source and image fields can be presented as

$$H_{y0}(x)e^{-i\omega t}=\int h(k_x)\exp[i(k_x x-\omega t)]dk_x$$

and

$$H(x)=\int h(k_x)T(k_x)\exp[ik_x x]dk_x,$$

respectively, with $T(k_x)$ being the transfer function. To find the transfer function, it is convenient to resort to the transfer matrix formalism.[8] The transfer matrix M relates the complex amplitudes of the incident and reflected waves to the ones on the opposite side of the one-dimensional (1D) system. For a given polarization, the 2×2 M matrix has elements m_{ij}. One can see that the transfer function is equal to $1/m_{22}$. The single-layer-lens transfer matrix, $M(l_1,d,l_2)$, corresponding to the pass from the source placed at $z=0$ to the image plane at $z=l_1+d+l_2$, is equal to the product $J_1(l_1)SJ_2(d)S^{-1}J_1(l_2)$, where

 ©2006 The American Physical Society

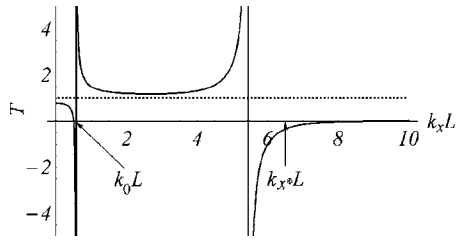

FIG. 1. The transfer function of a single-layer Pendry lens, $k_0L=0.5$.

$$S=\begin{Vmatrix} \frac{\zeta_2+\zeta_1}{2\zeta_2} & \frac{\zeta_2-\zeta_1}{2\zeta_2} \\ \frac{\zeta_2-\zeta_1}{2\zeta_2} & \frac{\zeta_2+\zeta_1}{2\zeta_2} \end{Vmatrix}, \quad J_i(l)=\begin{Vmatrix} \exp(ik_{zi}l) & 0 \\ 0 & \exp(-ik_{zi}l) \end{Vmatrix}$$

which takes into account Fresnel's formulas and "propagation" along the z axis.

Within the framework of the electrostatic approximation, the transfer function of a slab with $\varepsilon_2=-1$, $\mu_2=1$ is identically equal to unity.[3,4] Indeed, Eqs. (1) and (2) yield $(\zeta_1+\zeta_2)^2=0$ and $k_{z2}=k_{z1}=k_{z\ static}$. This makes the single-layer-lens transfer function,

$$T(k_x,l_1,L,l_2)=\frac{1}{m_{22}}=\frac{4\zeta_1\zeta_2\exp[ik_{z1}(l_1+l_2)]}{(\zeta_1+\zeta_2)^2\exp[-ik_{z2}L]-(\zeta_1-\zeta_2)^2\exp[ik_{z2}L]}, \tag{3}$$

equal to unity at $l_1+l_2=L$.

It should be remembered that large details will be restored with distortions, because the electrostatic approximation is not valid at low values of k_x ($k_x\sim k_0$) and the transfer function comes to depend on k_x (Fig. 1). Unfortunately, the transfer function tends to zero at $k_x\geqslant k_{x*}$, where k_{x^*} is a certain value depending on the properties of the lens and surrounding media (see Fig. 1 and Ref. 4). This phenomenon is associated with the inadequacy of the electrostatic approximation. At high values of k_x, the correction to the electrostatic value $(\zeta_1+\zeta_2)^2=0$ is still small; however, in Eq. (3), $(\zeta_1+\zeta_2)^2$ is multiplied by the exponentially large factor $\exp[-ik_{z2}L]\approx\exp[k_xL]$, which makes the transfer function (3) vanish at high values of k_x.

Besides the domain of high values of k_x ($k_x\geqslant k_{x^*}$), the deviation from the electrostatic approximation is observed near some points where the transfer function has singularities (see Fig. 1). It is the objective of this study to investigate the origin of these singularities and to determine the role they play in imaging.

II. THE STACKABLE PENDRY-RAMAKRISHNA LENS

It is well known that the resolution of the single-layer Pendry lens is restricted by losses (see Refs. 3 and 7). To decrease the losses, it was suggested in Ref. 4 to cut the silver slab into multiple thin layers separated by thin dielectric layers (see Fig. 2). Below, we follow Ref. 4 in assuming that the total thickness of the epsilon-negative layers L is the same for all values of N, so that the layers become thinner with increasing N.

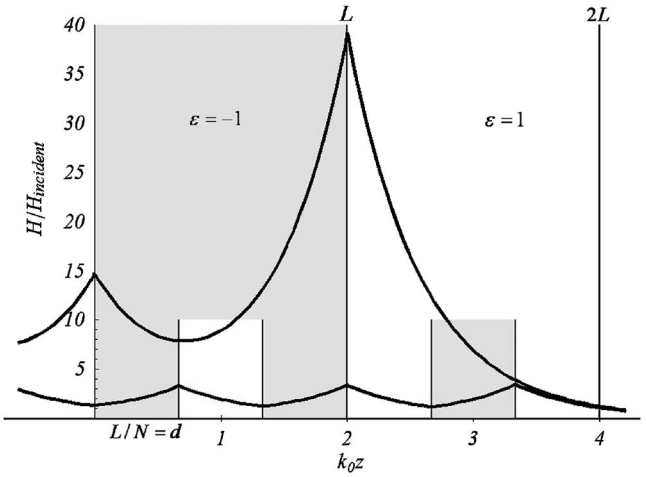

FIG. 2. The lens structures and the corresponding distributions of magnetic field for the single-layer (top structure and curve) and three-layer (bottom structure and curve) lenses. The gray and white layers have permittivities $\varepsilon_1=-1$ and $\varepsilon_2=1$, respectively, amplitudes of the incident wave are equal to unity in both cases; $k_0L=0.5$, $k_x/k_0=7$.

The analysis of a stackable lens in the electrostatic approach is similar to the analysis of the single-layer lens, Eqs. (1) and (2). The stackable-lens transfer matrix $M_N(l_1,l_2)$, describing the pass from the source placed at $z=0$ to the image plane at $z=l_1+(2N-1)d+l_2$, is equal to the product

$$J_1(l_1)SJ_2(d)S^{-1}(J_1(d)SJ_2(d)S^{-1})^{N-1}J_1(l_2).$$

In the electrostatic approach

$$S=\begin{Vmatrix} 0 & 1 \\ 1 & 0 \end{Vmatrix}=S^{-1}$$

and

$$J_1(l_1)SJ_2(d)S^{-1}=J_1(l_1)J_2^{-1}(d),$$

and as a result, $M_N(l_1,l_2)=J_1(l_1)J_1(l_2)J_1^{-1}(d)[J_1(d)J_2^{-1}(d)]^N$ and the transfer function is equal to $T_N(k_x,l_1,L,l_2)=\exp[ik_{z\ static}(l_1+l_2-d)]$.

Ultimately, we obtain an ideal image at a distance which meets the condition $l_1+l_2=d=L/N$. It is worth noting that the position of the image l_2 approaches the lens surface with the increase of N as $l_2=d-l_1=L/N-l_1$ (L is the total thickness of all metamaterial layers, and d is the thickness of one elementary layer). In particular, if we keep $l_1=l_2$, then $l_2=0.5L/N$, for $l_1=0$ we obtain $l_2=L/N$. This makes the stackable lens less promising for use in photolithography, where it is desirable to place the image as deep as possible into a layer of photoresist.[5,6] This displacement of the image is responsible for a decrease in the field amplitude. Indeed, the decay of the amplitude of the evanescent wave in the region behind the lens is independent of the lens structure. For producing an image, the strength of the field of this wave must have the

same value as that in the respective wave in the source. Because the distance between the image plane and the lens surface is shorter for the stackable lens, the amplitude of the field at its surface is lower (see Fig. 2).

It seems that, thanks to the lower field amplitude, the stackable lens can overcome a typical defect of a single-layer Pendry lens which is the sensitivity of the image quality to the energy dissipation[3,4] or, to be more precise, the presence of the imaginary parts of ε and/or μ. Because negative values of ε and μ are possible only in the materials exhibiting frequency dispersion, as follows from the Kramers-Kronig relations, nonzero imaginary parts are nearly always present. At first sight, the appearance of the imaginary part of the dielectric permittivity, $\varepsilon=\varepsilon'+i\varepsilon''$, primarily results in losses, which are proportional to $\varepsilon'' EE^*$ and are greater in the single-layer lens than in a stackable lens.

However, in Ref. 4, by means of a computer simulation, it was shown that the splitting a single-layer lens into N pieces leads to the improvement of the image even in the absence of losses. To understand this effect and the real cause for the image deterioration due to the imaginary part of the permittivity,[7] one has to employ a full-wave analysis.

First of all, this analysis shows that the appearance of ε'' primarily results not in the wave attenuation, which is proportional to $\exp[(\varepsilon'')^2 L(k_0/k_x)/\sqrt{1-\varepsilon' k_0^2/k_x^2}]$, but causes the waves' misphasing, which is linear in ε'' and proportional to the total thickness, L, of the metamaterials. Indeed, assuming that $\varepsilon'' \ll \varepsilon'$ we obtain[7]

$$k_z/k_0 \approx i\sqrt{k_x^2/k_0^2-\varepsilon'} + \frac{(k_0/k_x)}{\sqrt{1-\varepsilon' k_0^2/k_x^2}}\varepsilon'' + i\frac{(k_0/k_x)^3}{(1-\varepsilon' k_0^2/k_x^2)^{3/2}}(\varepsilon'')^2 + \ldots .$$

The consequence of this misphasing is the destructive interference that destroys the image. Hence, the reduction of the field amplitude and the energy dissipation, which accompany splitting the lens into parallel slices, is not the main effect that makes the lens performance better. There should be another mechanism that also works in the absence of losses.[4]

Secondly, in contrast to the electrostatic approach, the computer simulation[4] shows an existence of singularities of the transfer function.[4] The results of our simulation for a four-layer lens are shown in Fig. 3(a). This dependence of the transfer function on k_x resembles that of the single-layer lens with the only difference that the number of singularities increases. To analyze this dependence, it is useful to regard the stackable lens as a fragment of a photonic crystal (PC). Such an approach allows us to give a physical interpretation of all the features of the transfer function.

First, we can obtain the upper estimate for k_{x^*}. This can be done by treating a single-layer lens as a slab of the PC, which has a two-layer primitive cell consisting of a single-layer lens and a vacuum layer of the same thickness $d=L$. We can rewrite Eq. (3) in the form suitable for the interpretation in terms of the PC band structure. At high values of k_x, in the jth layer, we have $-ik_{zj}d=\kappa_j \approx k_x d>1$ and $\exp(\kappa_j) \approx 2\cosh(\kappa_j) \approx 2\sinh(\kappa_j)$. Then the transfer function (3) may be rewritten as

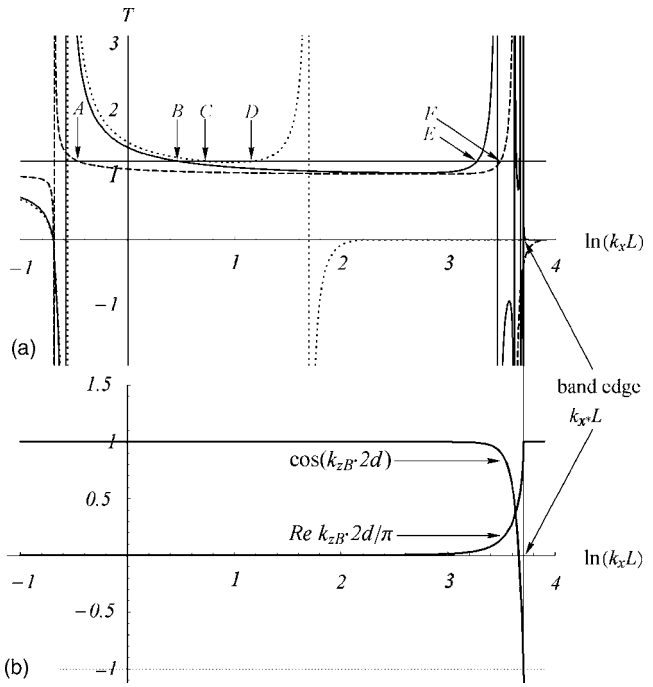

FIG. 3. (a) The transfer functions for a four-layer lens of the elementary layer thickness $L/4$ (solid line), a single-layer lens of the thickness L (dotted line), and a single-layer lens of the thickness $L/4$ (dashed line). The working ranges, where the deviation of the transfer function from unity is less than 20%, for each case are situated between the points B and E, C and D, A and F, respectively. $k_0L=0.5$. (b) $\cos(k_{zB}2d)$ and $\mathrm{Re}(k_{zB}2L/\pi)$ for the PC, corresponding to the solid and dashed lines in (a).

$$T \approx \frac{1}{2}\frac{1}{\cosh(\kappa_1)\cosh(\kappa_2)+\frac{1}{2}\left(\frac{\zeta_1}{\zeta_2}+\frac{\zeta_2}{\zeta_1}\right)\sinh(\kappa_1)\sinh(\kappa_2)}. \quad (4)$$

The denominator of T is equal to the right-hand side of the well-known dispersion equation for the Bloch wave number k_{zB} of a one-dimensional PC (see Ref. 9),

$$\cos 2k_{zB}d = \cos k_{z1}d\cos k_{z2}d - \frac{1}{2}\left(\frac{k_{z1}/\varepsilon_1}{k_{z2}/\varepsilon_2}+\frac{k_{z2}/\varepsilon_2}{k_{z1}/\varepsilon_1}\right)\sin k_{z1}d \sin k_{z2}d, \quad (5)$$

where the numerical subscripts denote the layer numbers in the primitive cell. Finally, Eq. (4) transforms into the following expression:

$$T \approx \frac{1}{2}\frac{1}{\cos 2k_{zB}L}. \quad (6)$$

In the band gap, $\cos 2k_{zB}L$ tends to infinity with an increase of k_x, which leads to vanishing of the transfer function. Although in the general case of the N-layer lens the expression for the transfer function T looks much more complicated than Eq. (3), we arrive at the same result: at $k_x > k_{x^*}$, the transfer function is almost equal to zero [see Figs. 3(a) and 3(b)]. Here and below, k_{x^*} denotes the upper estimate asso-

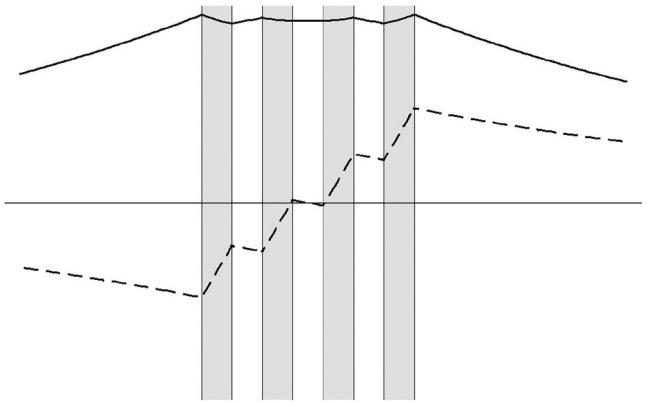

FIG. 4. Re(H_y) (solid line) and Im(E_x) (dashed line) distributions in the zero eigenstate ($n=0$) in a four-layer stackable lens.

ciated with the band edge $k_{zB}(k_{x*},k_0)$ of the PC. Thus, the interval where the transfer function markedly differs from zero is the PC conduction band. The size reduction of the PC cell brings the band edge $k_{zB}(k_{x*},k_0)$ to higher values of k_x (for comparison, in Fig. 3 we plot the transfer function of the original single-layer lens as in Fig. 1). This explains why it is advantageous to make the lens out of a larger number of layers if the total thickness is kept constant.[4]

In the case of the stackable lens, the electrostatic approximation becomes inadequate and image deterioration begins at smaller values of k_x and k_{zB} than the band edge values k_{x*} and $k_{zB}(k_{x*},k_0)$. The working range of imaging where the transfer function is close to unity is shown in Fig. 3(a) (the BE interval). This range is limited by the singularities of the transfer function. The transfer function of an N-layer lens has $N+1$ singularities enumerated and referred to as $n=0,1,\ldots,N$ [Fig. 3(a)]. Employing the PC approach, we can reveal their origin.

The distribution of the tangential magnetic field, $H_y(z)$, corresponding to these singularities is either an even or odd function with respect to the center of the lens (Figs. 4 and 5). In particular, the H_y distribution corresponding to the zeroth (Fig. 4) and the first [Fig. 5(a)] singularities are even functions. Starting with the first singularity, the symmetry of the

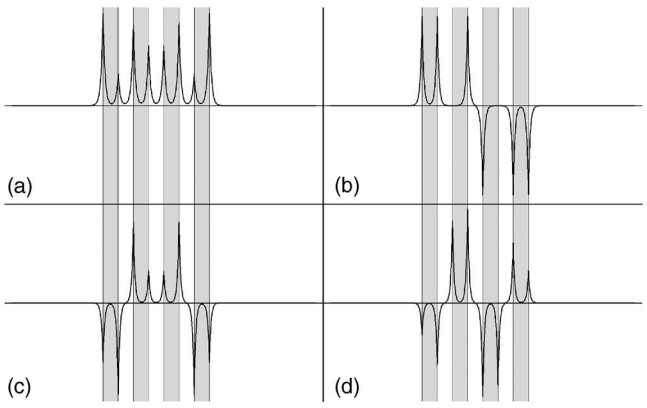

FIG. 5. A magnetic field distribution in the eigenstates of the four-layer stackable lens. The plots (a), (b), (c), and (d) correspond to $n=1$, 2, 3, and 4, respectively.

solutions alternates, with the simultaneous increase in the number of nodes of the solution by one (Fig. 5). The zeroth state violates this regularity. The reason is that the nature of the zero state is a volume plasmon resonance, whereas the remaining N states are modes of the PC resonator.

The zero singularity ($n=0$) of the transfer function of the stackable lens exists at $k_x=k_0(1+\delta)$ with $\delta \ll 1$, and the effective propagation constant (the Bloch wave number) k_{zB} is very small. At the frequency corresponding to $k_0L=0.5$, we have $k_{zB}L \sim 0.01\pi$,[10] so that the Bloch wave sees a homogenized medium which is an effective uniaxial crystal with $\varepsilon_{eff\,xx}=\varepsilon_{eff\,yy}=\langle\varepsilon\rangle=0$ and $\varepsilon_{eff\,zz}=1/\langle 1/\varepsilon\rangle=\infty$. When these conditions are satisfied, the excitation of a volume plasmon is possible. This plasmon differs from the well-known Langmuir plasmon where $D_z=0$, and $E_z\neq 0$. In our case, due to the relation $D_z=E_z/\langle 1/\varepsilon\rangle$, we have an anti-Langmuir plasmon with $D_z\neq 0$, $\langle E_z\rangle_z=0$. More precisely, the anti-Langmuir plasmon is TM polarized with $D_z(x)\neq 0$, $H_y(x)\neq 0$, $\langle E_z(x,z)\rangle_z=0$. Indeed, the Maxwell equations reduce to

$$\frac{d}{dx}H_y = ik_xH_y = -ik_0D_z,$$

$$\frac{d}{dz}E_x = ik_0H_y.$$

To construct an eigenstate for finite L, we have to match the solution inside the PC with two evanescent waves outside the PC slab. In these evanescent waves, the phase shift between the electric and magnetic fields is $\pm\pi/2$. A linear distribution of the electric field inside the PC, $E_x(z)=E_x(0)-iBz$, with constant B being in phase with H_y, satisfies the boundary conditions. In our discussion we set $k_{zB}=0$. In the exact solution, in an evanescent wave, $k_x=k_0(1+\delta)>k_0$ with nonzero $k_{zB}L\sim 0.01\pi$. Nevertheless, the field is distributed near $k_{zB}=0$ in the anti-Langmuir plasmon (see Fig. 4).

The position of the zeroth resonance depends slightly on N and d. Computer simulation shows that a decrease of d at fixed $L=Nd$ leads to a shift of the zeroth resonance to the left, $k_x\to k_0$, whereas the first resonance moves to the right. An increase of N at fixed d results in a shift of the zeroth resonance to the right [see Fig. 3(a)]. Simultaneously, the new PC resonator's mode arises. This mode shifts the $n=1$ singularity to the left [see Fig. 3(a)]. At some value of N, the zeroth and first singularities annihilate each other with consequent appearance of a new zeroth resonance.

Let us return to the remaining N eigensolutions (Fig. 5). They exist at the high values of k_x ($k_x \gg k_0$). Since the condition of total internal reflection in the vacuum layers is fulfilled, the local values of k_{iz} are purely imaginary quantities inside and outside the PC. The Bloch wave number, k_{zB}, however, is real (see Refs. 11–13). Under these conditions the Pendry lens can be treated as a resonator cavity for the traveling Bloch wave excited by the incident evanescent wave.[11]

The zero boundary conditions are fulfilled at infinity. For estimations, it seems reasonable to consider the resonator shown in Fig. 6. The walls are separated by a half-integer number $(N+1/2)$ of periods. The zero condition on the

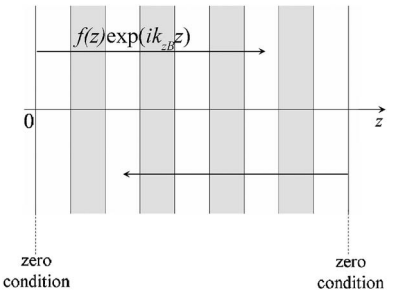

FIG. 6. A resonator formed by a stackable lens.

boundaries of the resonator (magnetic wall condition) means that $\sin[k_{zB}(2L+d)]=\sin[k_{zB}(2Nd+d)]=0$ or

$$k_{zB}2d(N+1/2)=\pi\cdot n \quad (n=1,2,\ldots,N), \tag{7}$$

which for large n and N are in a good agreement with an empirical law obtained in our computer simulation (see Fig. 7),

$$k_{zB}2d(N+1/2)=\pi\cdot(n-1/2) \quad (n=1,2,\ldots,N). \tag{8}$$

This equation can be obtained by taking into account the intracellular structure of the Bloch waves (see the Appendix).

The visible thickening of singularities in Fig. 3(a) is due to the nonlinear dependence of k_{nzB} on k_{nx}, Eq. (5) (n numerates eigenstates). The main features of the transfer function of stackable lenses with fixed L are summed up in Fig. 8. With increasing N we can see that (i) positions of resonances k_{nzB} (solid circles) are almost independent of N, (ii) the corresponding values of k_{nx} increase, (iii) the band edge $k_{zB}(k_{x*},k_0)$ slightly shifts to higher values, (iv) the number of resonances increases, and (v) the working range situated between the singularities with $n=0$ (volume plasmon resonance) and $n=1$ (the PC resonator mode) expands.

III. CONCLUSIONS

It seems reasonable to consider the first mode of the PC resonator as the upper limit of the working range. Indeed, the change of sign of the phasors causes destructive interference of different evanescent waves and destroys the image. This is the reason why we do not consider the domain with resonances to be the working range.

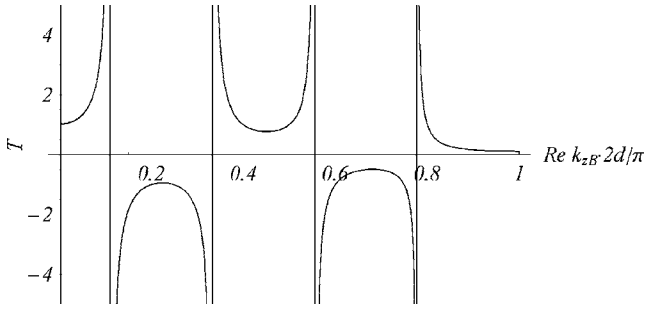

FIG. 7. The transfer function of a four-layer lens versus the Bloch wave number $\mathrm{Re}\,k_{zB}2d/\pi$. The vertical lines indicate the values of $k_{zB}2d/\pi=(2n-1)/(2N+1)$, $n=1,\ldots,N$. A point $k_{zB}2d/\pi=1$ corresponds to the band edge, $k_0L=0.5$.

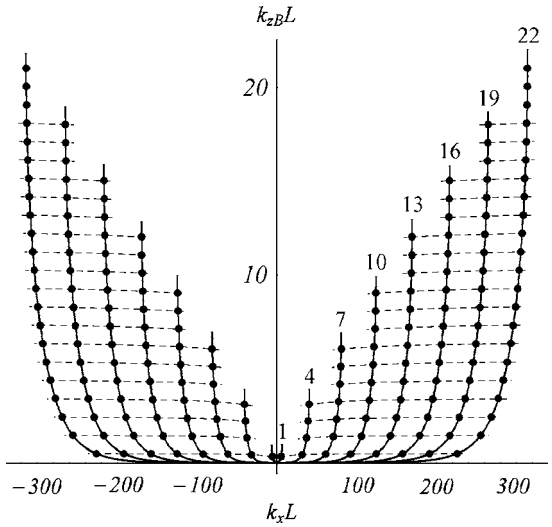

FIG. 8. The dependence of k_{zB} on k_x for different numbers of layers N at a fixed value of L (solid lines). The values of N are shown on the top ends of the curves. The curves terminate at the band edges. The solid circles indicate the eigenvalues of the PC resonator. The volume plasmon state is situated close to the coordinate origin. $k_0L=0.5$. The dashed lines connect the eigenvalues with the same n to illustrate a weak dependence of their position on N.

The division of the lens into parts without changing the total thickness of the material leads to an improvement of the image [see Fig. 3(a)]. For example, for a four-layer lens the working range, where the deviation of the transfer function from unity is less than 20%, expands from the interval CD to the interval BE [Fig. 3(a)]. Nevertheless, the single-layer lens made of one layer of the obtained photonic crystal works better than the whole crystal [the working range expands to the interval AF in Fig. 3(a)], because an addition of new layers of the fixed thickness d causes an increase of the total thickness L and shrinking of the working range. Indeed, as it follows from Eq. (8) for $n=1$,

$$k_{1zB}=\pi\frac{1/2}{2d(N+1/2)}=\frac{\pi}{4(L+d/2)}.$$

As was mentioned above, with an increase of N the zero singularity moves to the right (from A to B) whereas the first singularity moves to the left (from F to E). Therefore, an increase in the number N of the layers causes an expansion of the working range at fixed values of L and a reduction in this range at fixed values of d.

ACKNOWLEDGMENTS

This work was partly supported by the RF President Program "Leading Scientific Schools" (Grant No. NSh 1694.2003.02), RFBR Grants No. 04-02-16830, No. 05-02-19644, and No. 06-02-81053, and a CUNY Collaborative Grant No. 80209-0312.

APPENDIX

For high values of k_x the fields are rapidly vanishing while a wave moves away from the slab. Thus, it seems reasonable

to consider the field values to be equal to zero at a distance d from the slab (see Fig. 5). We arrive at the problem of the 1D resonator where the cavity includes the PC slab and the walls are magnetic (at the walls, the magnetic field is equal to zero). The length of the resonator is $2L+d$. The electromagnetic field inside the cavity is a sum of two Bloch waves traveling in opposite directions (see Fig. 6).

The magnetic field of the Bloch wave traveling in the positive z direction is $H_1(z)=f(z)\exp(ik_Bz)$. At the left boundary of the PC slab, we have $H_1(0)=f(0)=f_1$. Since $f(z)$ is a periodic function, $f(2d\cdot m)=f_1$ $(m=0,\ldots,N)$ and $H_1(2d\cdot m)=f_1\exp(ik_B2d\cdot m)$. Let us note that the walls are separated by a half-integer number of the crystal periods; therefore, the value of the periodic function on the right boundary differs from f_1. Let us denote it as $f_2=f(d+2dm)$ $(m=0,\ldots,N)$. Thus, $H_1[(2N+1)d]=f_2\exp[ik_B(2N+1)d]$.

Owing to the symmetry of the PC resonator, the value of the second Bloch wave $H_2(z)$ on the right boundary has the same magnitude as the value of the first Bloch wave on the left wall, that is $H_2[(2N+1)d]=\pm H_1(0)=\pm f_1$.

The sum of the magnetic fields of these Bloch waves is equal to zero on the walls of the PC resonator: $H_1[(2N+1)d]+H_2[(2N+1)d]=0$ or

$$f_2\cdot\exp[ik_B(2N+1)d]\pm f_1=0. \tag{A1}$$

One can see from Eq. (A1) that $|f_1|=|f_2|$ and $\exp[ik_B(2N+1)d]=\mp\exp i(\varphi_1-\varphi_2)$ with $\varphi_1=\arg(f_1)$, $\varphi_2=\arg(f_2)$, or

$$k_B(2N+1)d=\varphi_1-\varphi_2+\pi n,\quad n=0,1,2,\ldots\ . \tag{A2}$$

If the cavity were filled with uniform material, the solutions are usual plane waves $[f(z)=constant]$ and $\varphi_1-\varphi_2=0$, which leads to the ordinary resonance condition (7). Following Ref. 8 one can find the ratio

$$\frac{f_2}{f_1}=\frac{\zeta_1\dfrac{\exp(-ik_Bd)}{\sinh\kappa_1d}+\zeta_2\dfrac{\exp(ik_Bd)}{\sinh\kappa_2d}}{\zeta_1\coth\kappa_1d+\zeta_2\coth\kappa_2d}=\frac{\left(\dfrac{\zeta_2}{\sinh\kappa_2d}+\dfrac{\zeta_1}{\sinh\kappa_1d}\right)\cos(k_Bd)+i\left(\dfrac{\zeta_2}{\sinh\kappa_2d}-\dfrac{\zeta_1}{\sinh\kappa_1d}\right)\sin(k_Bd)}{\zeta_1\coth\kappa_1d+\zeta_2\coth\kappa_2d}=\alpha+i\beta.$$

At $k_x\gg k_0$, $k_xd\gg1$, $k_0d\sim1$, and $\varepsilon_1+\varepsilon_2=0$ we arrive at the following estimate:

$$\frac{\alpha}{\beta}=\frac{\dfrac{\sinh\kappa_1d}{\zeta_1}+\dfrac{\sinh\kappa_2d}{\zeta_2}}{\dfrac{\sinh\kappa_1d}{\zeta_1}-\dfrac{\sinh\kappa_2d}{\zeta_2}}\approx\frac{\varepsilon_1^2+\varepsilon_2^2}{\varepsilon_1-\varepsilon_2}\cdot\frac{1}{2}\left(\frac{k_0}{k_x}\right)^2(1-k_xd\coth k_xd)\ll1.$$

Thus the value of $f_1/f_2=\alpha+i\beta$ is an almost purely imaginary quantity. It means that a phase shift between f_1 and f_2 is approximately equal to $\pm\pi/2$ and we arrive at Eq. (8).

*Electronic address: a-vinogr@yandex.ru

[1] V. G. Veselago, Sov. Phys. Usp. **10**, 509 (1968).
[2] L. I. Mandel'stam, Zh. Eksp. Teor. Fiz. **15**, 475 (1945) (in Russian).
[3] J. B. Pendry, Phys. Rev. Lett. **85**, 3966 (2000).
[4] S. A. Ramakrishna, J. B. Pendry, M. C. Wiltshire, and W. J. Stewart, J. Mod. Opt. **50**, 1419 (2003).
[5] N. Fang, H. Lee, C. Sun, and X. Zhang, Science **308**, 534 (2005).
[6] M. M. Alkaisi, R. J. Blaikie, S. J. McNab, R. Cheung, and D. R. S. Cumming, Appl. Phys. Lett. **75**, 3560 (1999).
[7] A. P. Vinogradov and A. V. Dorofeenko, Opt. Commun. **256**, 333 (2005).
[8] M. Born and E. Wolf, *Principles of Optics* (Pergamon Press, Oxford, 1993).
[9] M. Rytov, Sov. Phys. Acoust. **2**, 71 (1956); Akust. Zh. **2**, 68 (1956).
[10] It should be noted that the Pendry crystal has a low-frequency band continuing up to the zero value of k_x.
[11] A. P. Vinogradov and A. V. Dorofeenko, J. Commun. Technol. Electron. **50**, 10 (2005).
[12] H. Jiang, H. Chen, H. Li, Y. Zhang, J. Zi, and S. Zhu, Phys. Rev. E **69**, 066607 (2004).
[13] A. Alù and N. Engheta, IEEE Trans. Antennas Propag. **51**, 2558 (2003).